https://doi.org/10.5194/egusphere-2026-180
Preprint. Discussion started: 17 March 2026

Desalinization-driven deep microbial reactivation destabilizes iron-bound carbon in coastal wetland restoration

Jingwen Gao[1], Pengcheng Jiang[1], Xiaofei Ye[1], Xingna Lin[1], Xuexin Shao[1], Ming Wu [1], Niu Li[1*]

[1] Wetland Ecosystem Research Station of Hangzhou Bay, State Key Laboratory of Wetland Conservation and Restoration, Zhejiang Provincial Key Laboratory of Wetland Intelligent Monitoring and Ecological Restoration, Research Institute of Subtropical Forestry, Chinese Academy of Forestry, Hangzhou 311400, China

*Corresponding author: Niu Li

Address: Research Institute of Subtropical Forestry, Chinese Academy of Forestry, Daqiao Road 73, Hangzhou, Zhejiang, 311400, China

E-mail addresses: Niuli@caf.ac.cn

Tel: +86 0571 63342931

Fax: +86 0571 63342931

Abstract

Tillage- and mulching-based interventions are increasingly used to control invasive plants and modify soil hydro-salinity, but their effects on subsoil carbon (C) stabilization are poorly quantified. We conducted an 18-month field experiment in a Spartina alterniflora–invaded estuarine wetland to compare plastic mulching (PM) and deep tillage (DT) and to resolve microbial–mineral controls on C across the 0–100 cm profile. PM induced pronounced, profile-wide desalinization (43–53% lower

https://doi.org/10.5194/egusphere-2026-180
Preprint. Discussion started: 17 March 2026

salinity) and a redistribution of microbial activity, increasing microbial biomass C in 30–100 cm soils by 25–61% while reducing activity in surface horizons. Relative to DT, PM was associated with much larger C depletion, with total C declining by 19–35% and the strongest SOC losses occurring at depth (up to ~65%). Carbon losses co-varied with weakened mineral protection, including 30–50% decreases in poorly crystalline Fe oxides (Feo) and 35–50% reductions in iron-bound organic carbon (Fe–OC). Amino-sugar biomarkers indicated coherent shifts in microbial necromass C with Fe–OC dynamics, suggesting vulnerability of long-lived, microbially derived subsoil C under rapid desalinization. Depth-resolved partial least squares path modeling showed contrasting dominant linkages by horizon: surface microbial communities aligned with SOC retention, whereas deep microbial properties covaried with iron mobilization and net C loss. Integrated across 0–100 cm, PM resulted in a net soil C decline of 65 ± 12 Mg C ha^{-1} over 18 months. These results highlight that mulching and tillage practices can have divergent subsoil C outcomes and that reactive Fe–C metrics are valuable for evaluating management impacts beyond the plough layer.

Keywords: Soil organic carbon; Iron-bound carbon; Microbial biomass; Desalinization; *Spartina alterniflora*; Blue carbon

1. Introduction

Coastal wetland soils sequester disproportionate amounts of organic carbon per unit area (up to 200 Mg C ha^{-1} in top meter), with 60-70% stored below 30 cm depth, protected by association with iron minerals and anaerobic conditions (Xia et al., 2022;

https://doi.org/10.5194/egusphere-2026-180
Preprint. Discussion started: 17 March 2026

Hao et al., 2024; Rogers et al., 2019). Invasion by *Spartina alterniflora* (*S.alterniflora*) has triggered widespread ecological restoration interventions, including mechanical removal and plastic mulching (PM), that fundamentally alter surface hydrology and salinity (Li et al., 2022; Wang et al., 2025). Yet restoration assessments focus almost exclusively on vegetation recovery and surface soil (0-30 cm) carbon dynamics (Yang et al., 2023; Zhang et al., 2022; Zhang et al., 2023), implicitly assuming that deeper horizons remain biogeochemically inert. This assumption leaves critical questions unanswered: Can management-induced changes in surface hydro-salinity propagate downward to activate subsurface microbial communities? And if so, what are the consequences for iron-mediated carbon stabilization mechanisms in deep soils?

The long-term stability of wetland soil carbon hinges on iron-organic associations formed under anaerobic conditions, where Fe(III)-reducing bacteria couple organic matter oxidation to iron oxide dissolution, paradoxically both mineralizing and stabilizing carbon depending on redox oscillations (Wang et al., 2022; Yu et al., 2021; Feng et al., 2025). This "Iron Gate" mechanism, wherein organo-Fe complexes resist microbial attack, is particularly prevalent in subsurface horizons where poorly crystalline ferrihydrite and reactive Fe(II) species accumulate (Jia et al., 2022; Wang et al., 2017). Salinity further modulates this system by suppressing microbial metabolic rates through osmotic stress, with halophilic taxa dominating at electrical conductivity >8 dS m^{-1} (Luo et al., 2025; Zhang et al., 2020). Traditional soil science posits that carbon metabolism declines exponentially with depth due to substrate depletion and physical isolation, rendering deep soils (>30 cm)

https://doi.org/10.5194/egusphere-2026-180
Preprint. Discussion started: 17 March 2026

biogeochemically dormant (Liu et al., 2022; Zheng et al., 2024). However, this paradigm derives largely from terrestrial systems and short-term laboratory incubations. In coastal wetlands, where profile-wide desalinization via freshwater infiltration or management interventions (e.g., PM) can alleviate osmotic constraints, the dormancy assumption remains untested. If deep microbial communities are merely osmotically suppressed, not substrate-limited, then desalinization could trigger a metabolic awakening, potentially mobilizing iron-protected legacy carbon via coupled geochemical dissolution and microbial iron reduction.

Despite the mechanistic understanding of iron-carbon coupling and microbial osmotic stress, three critical knowledge gaps preclude prediction of restoration impacts on deep soil carbon fate. First, nearly all studies of post-restoration biogeochemistry focus on 0-30 cm depth (Xiao et al., 2021; Li et al., 2021; Libbey and Hernández, 2021), leaving subsurface iron dynamics and microbial responses uncharacterized. Second, the spatial extent of desalinization effects, whether localized to mulch-covered surfaces or propagated through entire soil profiles, has not been quantified in field settings. Third, the relative contributions of abiotic iron oxide dissolution versus microbial iron reduction to Fe-OC destabilization remain unresolved, particularly under fluctuating redox-salinity conditions induced by management. Addressing these gaps is essential not only for refining wetland carbon budgets but also for identifying potential carbon costs of restoration that could offset vegetation-based sequestration gains. If common practices like PM inadvertently activate deep microbial reserves and destabilize iron-protected carbon, current

https://doi.org/10.5194/egusphere-2026-180
Preprint. Discussion started: 17 March 2026

restoration protocols may underestimate their climate impacts.

Here, we conducted a full-profile (0-100 cm) assessment of iron-carbon-microbe dynamics in a *S.alterniflora*-invaded coastal wetland 18 months after implementing two widely used restoration interventions: plastic mulching (PM, targeting moisture retention and weed suppression) and deep tillage (DT, enhancing physical disruption and aeration). We tested three specific hypotheses: (H1) PM-induced desalinization extends beyond surface layers to reduce osmotic stress in deep soils (30-100 cm), activating subsurface microbial communities as evidenced by increased microbial biomass and altered bacterial community structure. (H2) Desalinization triggers coupled geochemical dissolution and microbial reductive dissolution of reactive iron oxides (Feo, Fep), destabilizing Fe-bound organic carbon (Fe-OC) across the profile. (H3) The magnitude of carbon loss correlates with the spatial extent of desalinization and iron destabilization, with profile-wide effects under PM exceeding localized surface impacts under DT. By integrating sequential iron extraction, microbial biomass quantification, bacterial 16S rRNA profiling, and structural equation modeling, this study elucidates mechanistic linkages between restoration-induced environmental changes and deep soil carbon stability, providing process-based insights for designing climate-smart wetland management strategies.

2. Methods

2.1 Site Description and Experimental Design

The study was conducted in coastal wetlands of southern Hangzhou Bay

https://doi.org/10.5194/egusphere-2026-180
Preprint. Discussion started: 17 March 2026

(121°52′-121°25′E, 29°39′-30°21′N), Zhejiang Province, China, invaded by *Spartina alterniflora* since 1980s with > 85% coverage (Fug. 1). Soils are classified as typic sulfaquents with mean salinity of 12-18 dS m^{-1} in surface layers. The site experiences irregular semidiurnal tides (mean tidal range 2.5 m) and a subtropical monsoon climate (mean annual temperature 16.4°C, precipitation 1450 mm).

In June 2023, we established a randomized complete block design with three treatments: (1) Control (CK), unremediated *S. alterniflora* stands; (2) PM, 0.1 mm black polyethylene film applied after complete vegetation removal to suppress regrowth and reduce evaporative salt accumulation; and (3) DT, mechanical disruption to 160 cm depth using a rotary cultivator to enhance soil aeration and physical disturbance. Each treatment was replicated five times (n=5), with 20 m × 20 m plots separated by ≥50 m buffer zones to minimize edge effects.

Soil sampling was conducted in December 2024 (18 months post-treatment) using a 5 cm diameter stainless steel corer. At each plot, five cores (one central, four cardinal directions at 5 m from center) were collected and segmented into depth increments: 0-10, 10-20, 20-30, 30-50, and 50-100 cm. Samples from the same depth were homogenized to form one composite (≈500 g fresh weight), yielding 75 samples (3 treatments × 5 replicates × 5 depths). Samples were immediately transported to the laboratory on ice and divided into three aliquots: (i) fresh soil stored at 4°C for physicochemical and iron analyses (<2 mm sieving); (ii) air- dried soil (25°C, <0.25 mm) for total C/N and Fe-OC analyses; and (iii) frozen soil (-80°C) for DNA extraction.

https://doi.org/10.5194/egusphere-2026-180
Preprint. Discussion started: 17 March 2026

2.2 Soil Physicochemical Analyses

Soil pH and electrical conductivity (EC) were measured in 1:5 (w/v) soil-to-deionized water suspensions after 30 min end-over-end shaking at 25°C, using a glass electrode pH meter (PHSJ-3F, INESA, Shanghai, China) and conductivity meter (DDS-307, INESA), respectively. Gravimetric soil moisture was determined by oven-drying at 105°C for 24 h. Soil bulk density was measured using intact cores (100 cm^3) collected adjacent to sampling points, dried at 105°C, and weighed. Soil inorganic nitrogen (NH_4^+ and NO_3^-) was extracted from 5 g fresh soil with 50 mL of 2 M KCl by shaking at 200 rpm for 1 h at 25°C, followed by filtration (Whatman No. 42). Extracts were analyzed colorimetrically using a continuous-flow analyzer (AA3, SEAL Analytical, Germany) . Total carbon (TC) and nitrogen (TN) were determined using an elemental analyzer (Vario MAX CN, Elementar, Germany). Soil organic carbon (SOC) was estimated by loss-on-ignition (LOI) at 550°C for 4 h. Microbial biomass carbon (MBC) and nitrogen (MBN) were quantified using the chloroform fumigation-extraction method (Oren et al., 2018). Paired fresh soil samples (8 g, n=3 analytical replicates per composite) were either fumigated with ethanol-free chloroform in a vacuum desiccator for 24 h at 25°C or left non-fumigated. Both sets were extracted with 40 mL of 0.5 M K_2SO_4 by shaking for 30 min at 200 rpm, followed by centrifugation (4000 rpm, 10 min) and filtration (0.45 μm nylon). Organic C and total N in extracts were analyzed using a TOC/TN analyzer (TOC-L, Shimadzu, Japan). MBC and MBN were calculated as: MBC = EC / kEC and MBN = EN / kEN, where EC and EN are the differences in extracted C and N between

https://doi.org/10.5194/egusphere-2026-180
Preprint. Discussion started: 17 March 2026

fumigated and non-fumigated samples, and kEC = 0.45 and kEN = 0.54 are extraction efficiency factors (Joergensen, 1996; Brookes et al., 1985).

2.3 Iron Fractionation and Fe-bound Organic Carbon

Soil iron (Fe) pools were sequentially extracted following modified procedures of Poulton and Canfield (2005). Free Fe oxides (Fed, primarily crystalline hematite and goethite) were extracted by adding 40 mL of citrate-bicarbonate-dithionite (CBD) solution (0.27 M sodium citrate, 0.11 M sodium bicarbonate, 1 g sodium dithionite) to 1 g soil, heated in an 80°C water bath for 15 min with occasional stirring. Amorphous Fe oxides (Feo, mainly ferrihydrite and lepidocrocite) were extracted with 40 mL of 0.2 M ammonium oxalate/0.17 M oxalic acid (pH 3.0) in the dark at 25°C for 4 h with continuous end-over-end shaking. Organically complexed Fe (Fep) was extracted with 40 mL of 0.1 M sodium pyrophosphate (pH 10) by shaking for 16 h at 25°C. After each extraction, samples were centrifuged (4000 rpm, 10 min), and supernatants were filtered (0.45 μm) and acidified with 2% HNO_3 for storage. Iron concentrations in extracts were determined by inductively coupled plasma optical emission spectrometry (ICP-OES; iCAP 7400, Thermo Fisher Scientific, USA).

Fe-bound organic carbon (Fe-OC) was determined following Wagai and Mayer (2007) with modifications. Briefly, duplicate 1 g soil samples were treated with 40 mL of CBD solution (same composition as Fed extraction) at 25°C for 8 h in the dark to reductively dissolve Fe oxides and release associated OC. Control samples received 40 mL of 1 M NaCl solution (equivalent ionic strength) to account for OC loss via

https://doi.org/10.5194/egusphere-2026-180
Preprint. Discussion started: 17 March 2026

disprsion without Fe dissolution. After extraction, residues were washed three times with deionized water, freeze-dried, and ground to <0.25 mm. Organic C content in residues was measured using the elemental analyzer (Vario MAX CN). Fe-OC was calculated as:

$$\text{Fe-OC (g kg}^{-1}) = \text{OC\_control} - \text{OC\_CBD} \quad (1)$$

where OC_control and OC_CBD are organic carbon concentrations in control and CBD-treated residues, respectively. The proportion of Fe-associated OC (fFe-OC, %) was calculated as (Fe-OC / SOC) × 100.

2.4 Microbial Community Structure

Total genomic DNA was extracted from 0.5 g frozen soil using the E.Z.N.A.® Soil DNA Kit (Omega Bio-tek, USA) following manufacturer instructions. DNA quality was assessed by 1.0% agarose gel electrophoresis with GelRed staining, and concentration/purity were determined using a NanoDrop 2000 spectrophotometer (Thermo Fisher Scientific). The V4 hypervariable region of bacterial 16S rRNA gene was amplified using primers 515F (5′-GTGYCAGCMGCCGCGGTAA-3′) and 806R (5′-GGACTACNVGGGTWTCTAAT-3′). PCR reactions (25 μL) contained 12.5 μL 2× Phusion High-Fidelity PCR Master Mix (New England Biolabs), 0.5 μM each primer, and 20 ng template DNA. Amplification was performed in a T100 Thermal Cycler (Bio-Rad) using: initial denaturation at 95°C for 3 min; 27 cycles of 95°C for 30 s, 55°C for 30 s, 72°C for 30 s; final extension at 72°C for 10 min. Three technical replicates per sample were pooled, purified using the AxyPrep DNA Gel Extraction

https://doi.org/10.5194/egusphere-2026-180
Preprint. Discussion started: 17 March 2026

Kit (Axygen), and quantified by Qubit 4.0 Fluorometer (Invitrogen). Equimolar amounts (100 ng per sample) were pooled and sequenced on an Illumina MiSeq platform (2 × 300 bp paired-end) by Majorbio Bio-Pharm Technology Co. (Shanghai, China), targeting >50,000 raw reads per sample.

Raw sequences were processed using QIIME2 (v2022.11). Primers were removed with cutadapt (v4.1), and reads were quality-filtered (Q > 20), denoised, and merged using DADA2 with default parameters. Chimeric sequences were identified and removed using VSEARCH (v2.21.1). Amplicon sequence variants (ASVs) were taxonomically assigned using the SILVA database (v138, 99% similarity threshold). Samples were rarefied to 40,000 sequences per sample to normalize sequencing depth. ASVs classified as chloroplasts, mitochondria, or unassigned at domain level were excluded from downstream analyses.

2.5 Soil Organic Carbon Stock Calculations

SOC stocks were calculated using both fixed-depth (FD) and equivalent soil mass (ESM) approaches to account for potential bulk density changes under different treatments (Wendt and Hauser, 2013; Peng et al., 2024). The fixed-depth SOC stock (SOCS_FD, Mg C ha^{-1}) for each layer was:

$$SOCS\_FD_i = SOC_i \times BD_i \times D_i \times 0.1 \quad (2)$$

where SOC_i is organic carbon concentration (g kg^{-1}), BD_i is bulk density (g cm^{-3}), and D_i is layer thickness (cm) for the ith layer. The constant 0.1 converts units to Mg C ha^{-1}.

https://doi.org/10.5194/egusphere-2026-180
Preprint. Discussion started: 17 March 2026

2.6 Statistical Analyses

All data were tested for normality (Shapiro-Wilk test) and homogeneity of variance (Levene's test) prior to parametric analyses. When necessary, data were log or square root-transformed to meet assumptions. Effects of treatment and depth on individual variables (soil properties, iron pools, Fe-OC, microbial biomass, α-diversity indices) were assessed using two-way analysis of variance (ANOVA) with treatment and depth as fixed factors. Post-hoc pairwise comparisons were conducted using Duncan's test at $\alpha = 0.05$. All univariate analyses were performed in SPSS (v27.0, IBM Corp.). Bacterial community β-diversity was calculated using Bray-Curtis dissimilarity based on Hellinger-transformed ASV relative abundances to reduce the influence of rare taxa. Principal coordinates analysis (PCoA) was used for visualization, and treatment effects were tested using permutational multivariate analysis of variance (PERMANOVA) with 999 permutations. Relationships between microbial community structure and environmental variables were examined using Mantel tests (Spearman's correlation, 999 permutations). Pairwise Pearson correlations between dominant bacterial phyla and soil properties were calculated and visualized as heatmaps. All multivariate analyses were conducted in R (v4.3.1) using vegan (v2.6-4) and ggplot2 (v3.4.2) packages. Partial least squares path modeling (PLS-PM) was employed to quantify direct and indirect causal pathways linking restoration treatments to carbon stability. Path coefficients (β) were estimated using the pls-pm package (v0.4.9) with centroid weighting scheme and 1000 bootstrap iterations for significance testing. Model fit was evaluated using standardized root

https://doi.org/10.5194/egusphere-2026-180
Preprint. Discussion started: 17 March 2026

mean square residual (SRMR < 0.08) and Goodness of Fit (GoF > 0.70) as adequacy thresholds (Henseler et al., 2016). Separate models were constructed for surface (0-20 cm) and deep (30-100 cm) soils to test depth-dependent mechanisms. All figures were created using Origin Pro (2025, Origin Lab Corp.) and assembled in Adobe Illustrator (2024, Adobe Inc.). Statistical significance was declared at $P < 0.05$ unless otherwise stated, and data are presented as mean ± standard deviation (SD).

3. Results

3.1 Soil hydro-chemical properties and microbial biomass across depths

PM induced a profound reorganization of the soil's hydro-saline regime across the 0-100 cm profile, dismantling the vertical salinity gradients observed in CK. PM treatment triggered a striking profile-wide homogenization of moisture and salinity (P<0.05, Fig. 2a, d), with a dramatic 55%-60% and 54%-59% reduction in EC and salinity, respectively, in deep soils (30-100 cm, P<0.001, Fig. 2c). This deep-soil desalinization acted as a powerful environmental trigger, awakening a dormant microbial community and driving a 25%-110% surge in MBC in PM-treated deep soils, peaking at a remarkable 61% increase at 50-100 cm (P<0.001, Fig. 2i). In contrast, PM suppressed MBC in surface soils (0-30 cm, P<0.05), signaling a reversal of the soil's metabolic geography from surface-active to deep-dominated activity. DT, while reducing surface salinity by ~20% (P<0.05, Fig. 2c, d), had minimal impact on deep soils and uniformly reduced MBC by 9%-45% across the profile (P<0.05, Fig. 2i), underscoring PM's unique potency in activating a deep microbial reservoir. These

https://doi.org/10.5194/egusphere-2026-180
Preprint. Discussion started: 17 March 2026

shifts were accompanied by significant nitrogen pool restructuring, with PM causing the greatest TN loss (51%-74%) and altered distributions of NH_4^+ and NO_3^- compared to CK and DT (P<0.05, Fig. 2e-g).

3.2 Soil carbon pools and iron-associated carbon fractions

PM triggered a catastrophic collapse of soil carbon pools across the 0-100 cm profile by activating the deep microbial reservoir. TC and SOC declined by 19-35% and 34-65%, respectively, far exceeding DT losses (15-28% for TC, 25-35% for SOC, P<0.01, Fig. 3a-b). This was coupled with the failure of the 'Iron Gate,' where PM reduced Feo by 30-50% (P<0.01, Fig. 3g) and Fe-OC by 35-50% (P<0.001, Fig. 3c). SOCS-FD followed CK > DT > PM, with PM increasing SOCS-FD by 2.3 to 4.8 times at 50-100 cm (P<0.01, Fig. 3d). Fed declined under PM (CK > DT > PM in 0-50 cm; CK > PM > DT in 50-100 cm, P<0.05, Fig. 3d), while Fep shifted from PM > CK > DT in 0-30 cm to CK > PM > DT in 30-100 cm (P<0.05, Fig. 3e). The proportion of Fe-OC to SOC ($f_{Fe\text{-}OC}$) was higher in PM and DT than CK in 0-30 cm but dropped in 30-50 cm (DT > PM > CK, P<0.05, Fig. 3h). Vertical patterns showed uniform SOC in CK, depth-declining SOC in DT, and higher SOC at 50-100 cm in PM (Fig. 3b). Fe-OC was surface-enriched in CK, fluctuated in DT, and uniformly low in PM (Fig. 3c). SOCS-FD peaked at 50-100 cm across treatments (P<0.01, Fig. 3d), while Feo in PM declined with depth (P<0.05, Fig. 3g). DT increased $f_{F\text{-}eOC}$ by 10-30% in 0-50 cm (P<0.05, Fig. 3c), highlighting its less destructive impact.

3.3 Bacterial community composition and diversity

https://doi.org/10.5194/egusphere-2026-180
Preprint. Discussion started: 17 March 2026

PCoA revealed significant treatment-induced differentiation of bacterial community structure. At 0-10 cm depth, communities exhibited clear separation (PERMANOVA: $R^2 = 0.465$, $P < 0.001$; Fig. S1), with PM samples diverging from CK and DT along PC1 (explaining 28.48% of variance) and CK separating from DT along PC2 (23.49% of variance). Community differentiation intensified at 10-20 cm depth (PERMANOVA: $R^2 = 0.605$, $P < 0.001$), where treatments formed distinct clusters in multivariate space defined by PC1 (25.61%) and PC2 (21.06%).

Alpha diversity metrics indicated that PM reduced Shannon and Chao1 indices at 0-10 cm and 10-20 cm ($P < 0.05$; Supplementary Table S1), although no significant differences were detected. Venn diagram analysis identified 652 core amplicon sequence variants (ASVs) shared among all treatments at 0-10 cm, alongside treatment-specific ASVs numbering 3,482 (PM), 2,953 (CK), and 3,009 (DT; Fig. 4a). At 10-20 cm depth, 613 core ASVs were shared, with 3,400 (CK), 3,151 (DT), and 3,228 (PM) unique ASVs (Fig. 4b).

At the genus level, surface soil (0-10 cm) bacterial assemblages displayed treatment-specific taxonomic signatures. CK soils harbored elevated relative abundances of *Sulfurifustis* and *Acidibacter*, DT soils were enriched in *Nocardioides, unclassified Gemmatimonadaceae*, and *Nitrospira*, while PM soils were characterized by *Thiobacillus*, *Subgroup_22*, and *unclassified MBNT15 taxa*. At 10-20 cm depth, these patterns persisted, with additional increases in the relative abundances of *BD2-11 terrestrial group*, *Gammaproteobacteria*, and *Desulfobacterota* observed in both DT and PM treatments (Fig. 4c, d). Circos plots visualized broader taxonomic

https://doi.org/10.5194/egusphere-2026-180
Preprint. Discussion started: 17 March 2026

band widths and denser cross-sample connections for dominant genera in PM treatments, indicating enhanced community complexity (Fig. 4c, d).

3.4 Relationships between environmental factors and carbon dynamics

Mantel tests revealed strong, depth-dependent correlations between bacterial community structure and environmental factors (Fig. 5a-b). In surface soils (0-20 cm), salinity/electrical conductivity (SAL/EC) and the 'iron-carbon complex' (SOC, TC, MBC, TN, $f_{F\text{-}eOC}$, Feo, Fed) were the dominant drivers of community variation ($r \geq 0.4$, $P<0.01$), with SOC, TC, and $f_{F\text{-}eOC}$ showing strong positive inter-correlations ($r \approx 0.8\text{-}1.0$) and negative correlations with NO_3^-. Soil moisture and pH had weaker effects, particularly at 0-10 cm, but their influence increased at 10-20 cm. RDA corroborated these findings, explaining 74.73% of community variation at 0-10 cm, with PM samples distinctly separated along RDA1, driven by high pH and Fep versus low SOC, TC, and $f_{F\text{-}eOC}$ (Fig. S2).

PLS-PM (GOF=0.729, Fig. 5c-d) quantified the cascading pathways driving SOC depletion. PM strongly altered soil physicochemical conditions (β=-0.854, $P<0.001$) via profile-wide desalinization (EC reduced by 50%, Fig. 2c), destabilizing Fed (β=-0.344, $P<0.01$) and active iron phases (Fep/Feo, β=-0.312, $P<0.05$). These shifts indirectly amplified microbial decomposition, leading to substantial SOC (R^2=0.787) and Fe-OC (R^2=0.610) losses. In surface soils (0-20 cm), microbial communities positively influenced SOC (β=0.486, $P<0.05$) and Fe-OC (β=-0.184, $P<0.05$, Fig. 5e-f), reflecting taxa like *Thiobacillus* and *Desulfobacterota* (Fig. 4c-d)

https://doi.org/10.5194/egusphere-2026-180
Preprint. Discussion started: 17 March 2026

that stabilize carbon via anaerobic metabolism, contrasting with deep soil (30-100 cm) where desalinization and iron loss fueled carbon depletion.

4. Discussion

4.1 Deep-soil microbial reactivation challenges carbon stability paradigms

Our findings challenge the prevailing assumption that deep coastal wetland soils (>30 cm) function as metabolically quiescent, long-term carbon sinks (Wu et al.,2025). While this paradigm holds in many terrestrial systems, our 18-month field experiment demonstrates that PM, a common restoration tool, can reactivate deep-soil microbial communities through profile-wide desalinization, with profound consequences for carbon cycling.

PM induced dramatic salinity reductions (43-53% decrease in Salinity, 45-50% in EC) throughout the 0-100 cm profile (Fig. 2c, d), effectively homogenizing the hydro-chemical environment. This desalinization alleviated osmotic stress, a recognized constraint on microbial activity in saline soils (Huang et al., 2020; Zhang et al., 2024; Wang et al., 2025), triggering a 25-61% increase in MBC in deep soils (30-100 cm), with peak enhancement at 50-100 cm depth (Fig. 2h). Simultaneously, PM suppressed surface-soil MBC (0-30 cm), inverting the typical depth gradient of microbial activity from surface-dominated to deep-enhanced. This metabolic redistribution contrasts sharply with DT, which uniformly reduced MBC by 10-20% across all depths without activating deep communities, underscoring that profile-wide desalinization, not physical disturbance drives deep microbial reactivation.

https://doi.org/10.5194/egusphere-2026-180
Preprint. Discussion started: 17 March 2026

This observation aligns with emerging evidence that environmental shifts can unlock previously inactive microbial reservoirs (Sainjan et al., 2019; Huang et al., 2020; Hernandez et al., 2021), though few studies have documented such responses in coastal wetlands. The activated deep microbiome likely includes facultative anaerobes and halotolerant taxa adapted to fluctuating redox and salinity conditions, as suggested by increased relative abundance of *Gammaproteobacteri*a and *Desulfobacterota* in PM-treated deep soils (Fig. 4c, d). However, direct functional evidence via metagenomics or activity assays is needed to confirm their metabolic roles.

The implications extend beyond single-site observations. If deep microbial reactivation occurs broadly under desalinization-driven restoration, current carbon accounting frameworks, which predominantly focus on surface horizons (0-30 cm), may systematically underestimate carbon vulnerability (Wen et al., 2023; Chen et al., 2018). Our results suggest that full-profile (0-100 cm minimum) monitoring is essential for accurate assessment of restoration carbon balance, particularly in saline coastal systems where osmotic constraints naturally suppress deep microbial activity.

Sainjan, N., Chinnasamy, S., Ramachandran, P., Robin, R., and Ramachandran, R., 2019. Oil-Spill Triggered Shift in Indigenous Microbial Structure and Functional Dynamics in Different Marine Environmental Matrices. Scientific Reports, 9. https://doi.org/10.1038/s41598-018-37903-x.

4.2 Iron-mediated carbon destabilization: coupled geochemical and microbial

https://doi.org/10.5194/egusphere-2026-180
Preprint. Discussion started: 17 March 2026

processes

The substantial carbon losses observed under PM (19-35% for TC, 38-65% for SOC; Fig. 3a, b) were tightly coupled with destabilization of Fe-OC, a key mechanism for long-term carbon preservation in anaerobic soils (Wu et al., 2025; Ni et al., 2024). PM reduced poorly crystalline Feo by 30-50% and Fe-OC by 35-50% (Fig. 3c, g), substantially exceeding losses under DT. This iron-carbon decoupling likely involves both abiotic and biotic pathways.

Geochemically, profile-wide desalinization may have enhanced the solubility and mobility of reactive Fe(III) phases through ionic strength reduction and pH shifts, promoting reductive dissolution under the prevailing anaerobic conditions (Wang et al., 2025; Yang et al., 2021). The pronounced decline in Feo, the most bioavailable iron fraction, supports this mechanism (Fig. 3g). Biologically, the activated deep microbial community may include iron-reducing bacteria (suggested by increased *Desulfobacterota* abundance; Fig. 4c, d), which couple Fe(III) reduction to organic carbon oxidation, releasing both CO_2 and soluble Fe(II) (Zhao et al., 2024; Lovley and Phillips, 1988). Our PLS-PM quantitatively supports this cascade: PM-induced physicochemical changes directly destabilized Feo, and Fep/Feo, iron pools, which in turn drove substantial losses of SOC and $f_{Fe\text{-}OC}$ (Fig. 5c, d). Alternative mechanisms warrant consideration. Fe-OC losses could result from leaching of dissolved Fe(II)-organic complexes following reductive dissolution, rather than complete mineralization to CO_2 (Daugherty et al., 2017). Without pore water chemistry data,

https://doi.org/10.5194/egusphere-2026-180
Preprint. Discussion started: 17 March 2026

we cannot definitively partition Fe-OC fate between microbial respiration and lateral export. Additionally, the observed patterns may reflect redistribution rather than net loss across the full soil profile, though our depth-integrated stocks suggest genuine depletion (Fig. 3d).

Depth-stratified PLS-PM models revealed contrasting microbial-carbon relationships. In surface soils (0-20 cm), bacterial communities positively influenced SOC and $f_{Fe\text{-}OC}$ (Fig. 5e, f), potentially reflecting carbon-stabilizing activities of sulfur-cycling taxa (*Thiobacillus*) and iron-metabolizing groups (*Desulfobacterota*) under microaerobic conditions (Berg et al., 2019). This contrasts with deep soils (30-100 cm), where desalinization-induced iron mobilization and enhanced microbial decomposition synergistically fueled carbon depletion, underscoring depth-dependent regulation of carbon stability. Notably, DT maintained 10-22% higher $f_{Fe\text{-}OC}$ than PM in surface soils (0-50 cm; Fig. 3h), suggesting that physical disturbance without profile-wide desalinization minimizes iron-mediated carbon destabilization. This distinction highlights that the magnitude and spatial extent of geochemical perturbation, not disturbance intensity alone, determine iron-carbon coupling resilience.

4.3 Carbon balance implications for coastal wetland restoration

Quantifying the full carbon consequences of restoration requires integrating soil stock changes with vegetation carbon dynamics over relevant timescales. PM reduced total carbon stocks by about 65 Mg C ha^{-1} across the 0-100 cm profile over 18 months

https://doi.org/10.5194/egusphere-2026-180
Preprint. Discussion started: 17 March 2026

(calculated from depth-weighted TC losses and measured bulk density; see Methods), equivalent to an annual depletion rate of ~43 Mg C ha^{-1} yr^{-1}. To contextualize this loss, aboveground biomass carbon in restored coastal wetlands typically accumulates at 1-3 Mg C ha^{-1} yr^{-1} following native vegetation re-establishment (Zheng et al., 2025; Rowland et al., 2024). If sustained, our observed soil carbon depletion would require 15-43 years of vegetation carbon uptake to offset, assuming no further deep-soil losses and successful plant community recovery.

This temporal imbalance raises concerns about net ecosystem carbon balance, particularly if PM-induced soil carbon losses continue beyond the initial 18-month period captured in our study. Three trajectories are plausible: (1) stabilization as labile carbon pools are exhausted; (2) deceleration if native vegetation establishment enhances fresh carbon inputs that outpace deep-soil decomposition; or (3) sustained loss if Fe-OC depletion progressively exposes more recalcitrant carbon fractions to microbial attack. Without multi-year monitoring and direct measurements of CO_2 and CH_4 fluxes, we cannot definitively assess whether PM-treated sites function as net carbon sources or sinks at the ecosystem-atmosphere interface.

Our findings align with growing recognition that restoration interventions can inadvertently mobilize legacy soil carbon stocks, generating restoration carbon debts that offset vegetation-based sequestration gains (Ascenzi et al., 2025; Bhan et al., 2025). In coastal wetlands, which store disproportionately large carbon stocks, such losses could substantially impact regional carbon budgets. For example, if extrapolated to the ~16,000 ha of *S. alterniflora* invaded wetlands in the Yangtze

https://doi.org/10.5194/egusphere-2026-180
Preprint. Discussion started: 17 March 2026

estuary alone (Gan et al., 2009), PM-induced soil carbon losses could total 0.7-1.1 Tg C, equivalent to 2.5-3.8Tg CO_2, comparable to annual emissions from a mid-sized city.

These results necessitate re-evaluation of restoration carbon accounting frameworks. Current blue carbon protocols and national greenhouse gas inventories often emphasize vegetation biomass and surface-soil (0-30 cm) changes (Murdiyarso et al., 2023; Asanopoulos et al., 2021), potentially overlooking deep-soil carbon vulnerability. We recommend that restoration carbon assessments incorporate: (1) full-profile soil carbon monitoring (0-100 cm minimum); (2) iron-associated carbon metrics (Fe-OC, $f_{Fe\text{-}OC}$) as early indicators of carbon destabilization; and (3) multi-year (≥5 years) flux measurements to capture carbon trajectory stabilization. Integrating these metrics into carbon credit verification protocols and climate mitigation strategies will help ensure that coastal restoration investments achieve genuine, long-term climate benefits.

4.4 Research priorities and knowledge gaps

Several limitations of our study define critical priorities for future research. First, our 18-month dataset captures only the initial restoration response phase. Multi-year (≥5 years) monitoring is essential to assess whether carbon losses stabilize, accelerate, or reverse as ecosystems mature. Second, the absence of direct greenhouse gas flux measurements precludes definitive conclusions about net ecosystem carbon balance. Depth-resolved CO_2 and CH_4 flux monitoring, coupled with pore water

https://doi.org/10.5194/egusphere-2026-180
Preprint. Discussion started: 17 March 2026

dissolved organic carbon analysis, is needed to close the carbon budget and partition losses between atmospheric efflux and lateral export. Third, our single-site study in a Yangtze estuary wetland may not generalize to other coastal settings with differing baseline salinity, vegetation types, or hydrological regimes. Comparative studies across regional gradients are necessary to identify thresholds where desalinization-induced carbon losses emerge.

Mechanistically, the microbial functional repertoire orchestrating deep-soil carbon mineralization and iron reduction remains uncharacterized. Integrated metagenomics and metatranscriptomics approaches targeting functional genes, including iron reductases (mtrC, cymA), organic carbon depolymerases, and respiratory pathways, would definitively identify the microbial actors and biochemical mechanisms driving iron gate failure. Complementary measurements of depth-resolved redox potential, Fe(II)/Fe(III) speciation, and microbial respiration rates would validate hypothesized iron-carbon-microbe linkages.

Finally, translating site-specific observations into predictive capacity requires process-based modeling. Incorporating mechanisms of osmotic stress relief, iron oxide dynamics, and depth-dependent microbial activity into existing frameworks (e.g., Wetland-DNDC, DAYCENT) would enable scenario analysis of restoration strategies under varying environmental conditions. Such models could identify management practice, such as controlled desalinization rates, phased tillage approaches, or iron amendment, that balance invasive species control with carbon stock preservation, ultimately informing climate-smart coastal restoration at regional

https://doi.org/10.5194/egusphere-2026-180
Preprint. Discussion started: 17 March 2026

to global scales.

5. Conclusion

Plastic mulching induced strong profile-wide desalinization in an invaded coastal wetland and was associated with a pronounced reorganization of belowground carbon (C) processes across the 0–100 cm soil profile. Relative to deep tillage, mulching coincided with greater whole-profile C depletion, with total C declining by 19–35% and the strongest SOC losses occurring in deep horizons (up to ~65%). Deep soils (30–100 cm) showed increased microbial biomass C (+25–61%), suggesting enhanced microbial activity under desalinized conditions. Carbon losses co-occurred with weakened mineral protection, evidenced by coupled declines in poorly crystalline Fe oxides (Feo; 30–50%) and Fe-bound organic carbon (Fe–OC; 35–50%). Amino-sugar biomarkers indicated coherent shifts in microbial necromass C with Fe–OC dynamics, highlighting potential vulnerability of long-lived, microbially derived C fractions in subsoils. Depth-resolved path modeling further emphasized horizon-specific linkages: surface microbial attributes aligned more closely with SOC retention, whereas deep microbial attributes covaried with iron mobilization and SOC loss. Integrated across 0–100 cm, mulching was associated with a net soil C decline of 65 ± 12 Mg C ha^{-1} over 18 months. These findings show that mulching and tillage choices can lead to contrasting subsoil C outcomes, supporting the need for profile-resolved monitoring and reactive Fe–C metrics to evaluate management impacts beyond the surface layer.

https://doi.org/10.5194/egusphere-2026-180
Preprint. Discussion started: 17 March 2026

493 **Figures**

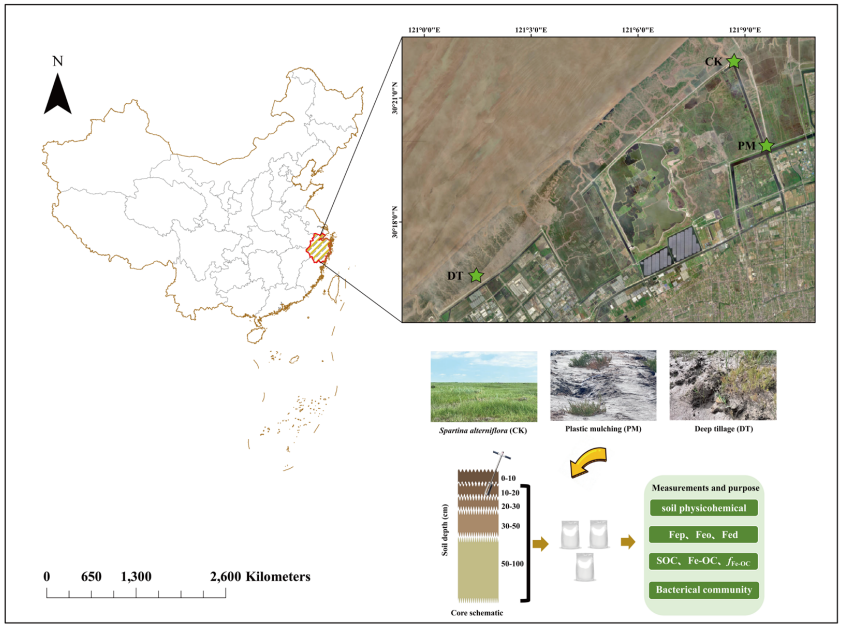

494

495 **Fig. 1** Geographic location and sampling design of the study area in the coastal
496 wetlands of Hangzhou Bay, Zhejiang province China. The three sampling sites
497 represent different *Spartina alterniflora* management regimes: CK, unremediated
498 *Spartina alterniflora* (control); PM, *S. alterniflora* removal followed by plastic
499 mulching; and DT, *S. alterniflora* removal followed by deep tillage.
500 note: basemap/satellite imagery was obtained from Tianditu (National Platform for
501 Common Geospatial Information Services, China), accessed on 25 September 2025.
502 The downloaded imagery did not provide a standard-map approval number or detailed
503 attribution; therefore, the platform name and access date are provided here. The
504 sampling locations were plotted and the map was composed in GIS software.

https://doi.org/10.5194/egusphere-2026-180
Preprint. Discussion started: 17 March 2026

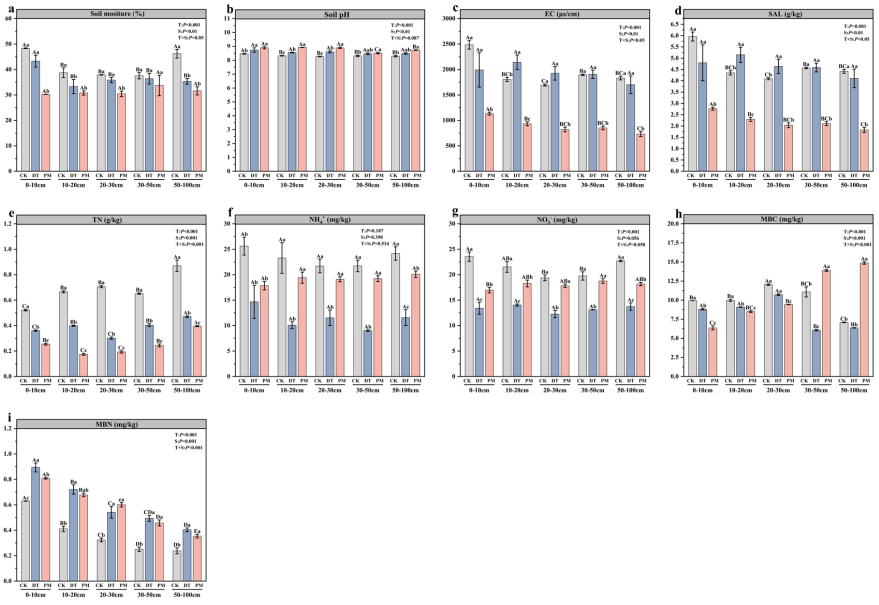

Fig. 2 Soil physicochemical properties under different management treatments.(a) Soil moisture, (b) pH, (c) electrical conductivity (EC), (d) salinity (SAL), (e) total nitrogen(TN), (f) ammonium (NH_4^+), (g) nitrate (NO_3^-), (h) microbial biomass carbon (MBC), and (i) microbial biomass nitrogen (MBN) across soil profiles under CK (control), DT (deep tillage), and PM (plastic mulching) treatments. Bars represent the mean ± standard error, and lowercase letters above the bars significant differences between treatments at the same soil depth ($P < 0.05$), while uppercase letters indicate significant differences between soil depths within the same treatment ($P < 0.05$).

https://doi.org/10.5194/egusphere-2026-180
Preprint. Discussion started: 17 March 2026

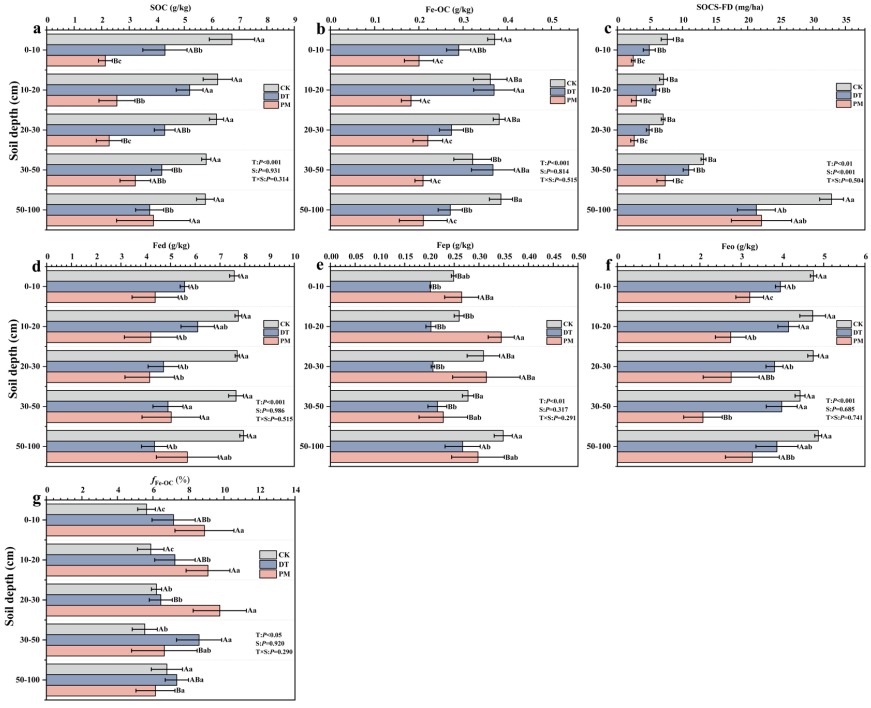

Fig. 3 Soil carbon and iron dynamics across soil profiles under different treatments. (a) Total carbon (TC), (b) soil organic carbon (SOC), (c) iron-bound organic carbon (Fe-OC), (d) soil carbon storage flux (SOCS-FD), (e) free iron (Fep), (f) iron-extractable Fe (Fed), (g) iron oxides (Feo), (h) proportion of iron-bound organic carbon ($f_{Fe\text{-}OC}$%) across different soil depths under CK (control), DT (deep tillage), and PM (plastic mulching) treatments. Bars represent the mean ± standard error, and lowercase letters above the bars indicate significant differences between treatments at the same soil depth ($P < 0.05$), while uppercase letters indicate significant differences between soil depths within the same treatment ($P < 0.05$).

https://doi.org/10.5194/egusphere-2026-180
Preprint. Discussion started: 17 March 2026

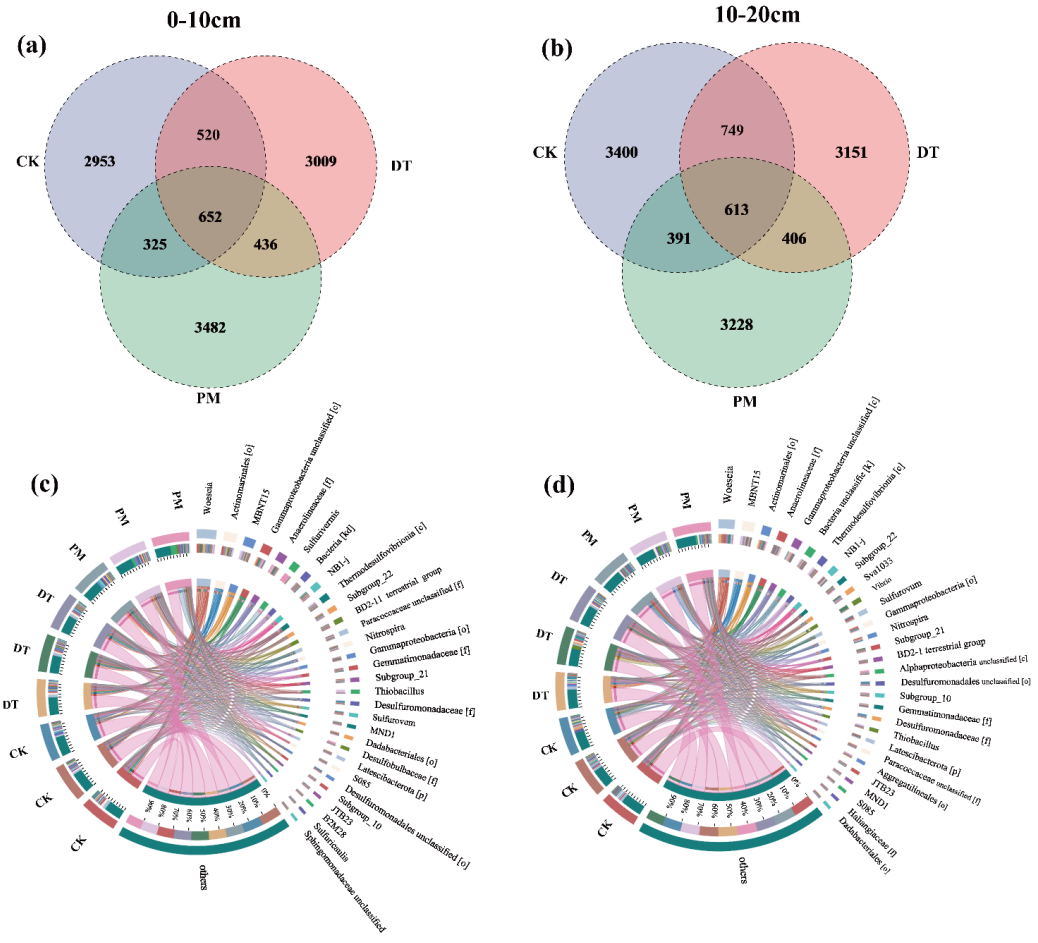

Fig. 4 Taxonomic composition and treatment-specific shifts in soil bacterial communities. (a, b) Venn diagrams showing the numbers of shared and unique amplicon sequence variants (ASVs) among CK (control), DT (deep tillage), and PM (plastic mulching) treatments in the 0–10 cm (a) and 10–20 cm (b) soil layers. (c, d) Circos plots depicting the relative abundance and treatment connectivity of dominant bacterial genera in the 0–10 cm (c) and 10–20 cm (d) soil layers under CK, DT, and PM treatments.

https://doi.org/10.5194/egusphere-2026-180
Preprint. Discussion started: 17 March 2026

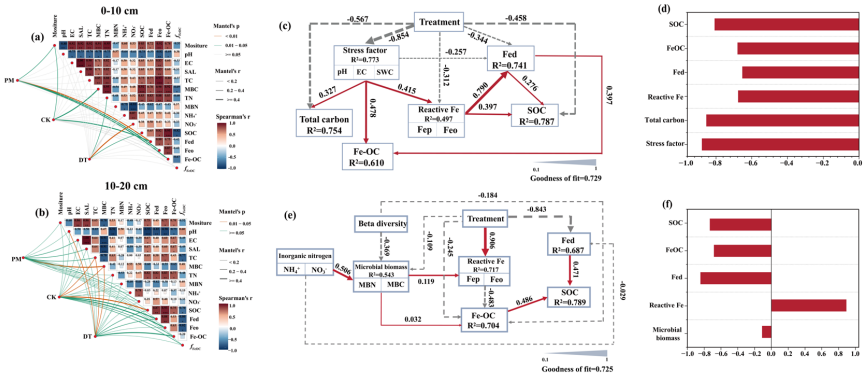

Fig. 5 Mantel tests and partial least squares path models (PLS-PM) linking soil environmental variables, bacterial communities and soil carbon under different *S. alterniflora* management regimes. (a, b) Mantel tests between bacterial community composition (Bray–Curtis dissimilarity) and environmental variables at (a) 0–10 cm and (b) 10–20 cm soil depths; arrows indicate significant drivers (Mantel's r ≥ 0.4, $P < 0.01$). (c) PLS-PM showing direct and indirect effects of management, environmental stress and reactive iron pools on soil carbon fractions. (d) Standardized total effects of each component on iron-bound organic carbon (Fe–OC) derived from the model in (c). (e, f) PLS-PM for surface soils (0–20 cm) including bacterial community attributes to evaluate microbial mediation of Fe–OC and other carbon pools; model conventions are as in (c, d). SAL, salinity; EC, electrical conductivity; SOC, soil organic carbon; TC, total carbon; MBC, microbial biomass carbon; TN, total nitrogen; Fe–OC, iron-bound organic carbon; Fep, free iron; Feo, oxidizable iron; Fed, dithionite-extractable iron.

Acknowledgments

We would like to acknowledge the assistance of Zhu Xiaohong from the Wetland Ecosystem Research Station of Hangzhou Bay for her support in field sampling.

Funding

https://doi.org/10.5194/egusphere-2026-180
Preprint. Discussion started: 17 March 2026

Fundings for this project was provided by Fundamental Research Funds of CAF (CAFYBB2024MA029); Open Fund for the Wetland Water Resources Research and Conservation Project from Hangzhou Normal University(HZNU-KFJJ2025)；Pioneer and Leading Goose R&D Program of Zhejiang (2025C02050; 2025C02230) and National Key Research and Development Program of China (2023YFE0101700)；the Pioneer and Leading Goose R&D Program of Zhejiang Province (Grant No. 2024C02002)，the Key R&D Program of Zhejiang (2024C03236)

Conflict of interest

The authors declare that they have no known competing financial interests or personal relationships that could have appeared to influence the work reported in this paper.

Author contributions

Jingwen Gao: Writing-original draft, Visualization, Software, Methodology Investigation, Formal analysis. **Pengcheng Jiang**: Software, Methodology, Investigation **Xiaofei Ye**: Investigation, **Xingna Lin**: Investigation. **Xuexin Shao**: Investigation. **Ming Wu**: Supervision, Investigation and Funding acquisition. **Niu Li:** Writing-review & editing, Validation, Supervision, Software, Resources, Project administration, Investigation, Funding acquisition.

Data availability

Raw data of the study in Wetland Ecosystem Research Station of Hangzhou Bay are available at https://pan.baidu.com/s/1GfHljucHF6jOfE8e4WXz3w

https://doi.org/10.5194/egusphere-2026-180
Preprint. Discussion started: 17 March 2026

572 **Reference**

573 Ascenzi, I., Hilbers, J., van Katwijk, M. M., Huijbregts, M. A. J., and Hanssen, S. V.:
574 Increased but not pristine soil organic carbon stocks in restored ecosystems, Nature
575 Communications, 16, 637, https://doi.org/10.1038/s41467-025-55980-1, 2025.
576 Asanopoulos, C. H., Baldock, J. A., Macdonald, L. M., and Cavagnaro, T. R.:
577 Quantifying blue carbon and nitrogen stocks in surface soils of temperate coastal
578 wetlands, Soil Res., 59, 619–629, https://doi.org/10.1071/SR20040, 2021.
579 Bhan, M., Misher, C., Hiremath, A., and Vanak, A. T.: Restoration maintains high
580 soil carbon stocks in Asia's largest tropical grassland, Ecological Applications, 35,
581 e70073, https://doi.org/10.1002/eap.70073, 2025.
582 Berg, J. S., Jézéquel, D., Duverger, A., Lamy, D., Laberty-Robert, C., and Miot, J.:
583 Microbial diversity involved in iron and cryptic sulfur cycling in the ferruginous,
584 low-sulfate waters of Lake Pavin, PLoS ONE, 14, e0212787,
585 https://doi.org/10.1371/journal.pone.0212787, 2019.
586 Brookes, P. C., Landman, A., Pruden, G., and Jenkinson, D. S.: Chloroform
587 fumigation and the release of soil nitrogen: A rapid direct extraction method to
588 measure microbial biomass nitrogen in soil, Soil Biology and Biochemistry, 17, 837–
589 842, https://doi.org/10.1016/0038-0717(85)90144-0, 1985.
590 Chen, S., Wang, F., Zhang, Y., Qin, S., Wei, S., Wang, S., Hu, C., and Liu, B.:
591 Organic carbon availability limiting microbial denitrification in the deep vadose zone,
592 Environmental Microbiology, 20, 980–992, https://doi.org/10.1111/1462-2920.14027,
593 2018.
594 Daugherty, E. E., Gilbert, B., Nico, P. S., and Borch, T.: Complexation and redox
595 buffering of iron (II) by dissolved organic matter, Environmental Science &
596 Technology, 51, 11096–11104, https://doi.org/10.1021/acs.est.7b03152, 2017.
597 Feng, X., Zhao, Y., Wang, H., and Liu, C.: Iron–organic carbon interactions in
598 wetlands: Implications for wetland carbon preservation under global changes, Global
599 Change Biology, 31, e70300, https://doi.org/10.1111/gcb.70300, 2025.
600 Hao, Q., Song, Z., Zhang, X., He, D., Guo, L., van Zwieten, L., Yu, C., Wang, Y.,

https://doi.org/10.5194/egusphere-2026-180
Preprint. Discussion started: 17 March 2026

Wang, W., Fang, Y., Fang, Y., Liu, C.-Q., and Wang, H.: Organic blue carbon sequestration in vegetated coastal wetlands: Processes and influencing factors, Earth-Sci. Rev., 255, 104853, https://doi.org/10.1016/j.earscirev.2024.104853, 2024.

Hernandez, D. J., David, A. S., Menges, E. S., Searcy, C. A., and Afkhami, M. E.: Environmental stress destabilizes microbial networks, ISME Journal, 15, 1722–1734, https://doi.org/10.1038/s41396-020-00882-x, 2021.

Huang, L., Zhang, G., Bai, J., Xia, Z., Wang, W., Jia, J., Wang, X., Liu, X., and Cui, B.: Desalinization via freshwater restoration highly improved microbial diversity, co-occurrence patterns and functions in coastal wetland soils, Science of the Total Environment, 765, 142769, https://doi.org/10.1016/j.scitotenv.2020.142769, 2021.

Jia, Z., Huang, X., Li, L., Li, T., Duan, Y., Ling, N., and Yu, G.: Rejuvenation of iron oxides enhances carbon sequestration by the "iron gate" and "enzyme latch" mechanisms in a rice–wheat cropping system, Science of the Total Environment, 839, 156209, https://doi.org/10.1016/j.scitotenv.2022.156209, 2022.

Joergensen, R. G. and Mueller, T.: The fumigation-extraction method to estimate soil microbial biomass: Calibration of the kEN value, Soil Biology and Biochemistry, 28, 33–37, 1996.

Li, H., Mao, D., Wang, Z., Huang, X., Li, L., and Jia, M.: Invasion of Spartina alterniflora in the coastal zone of mainland China: Control achievements from 2015 to 2020 towards the Sustainable Development Goals, Journal of Environmental Management, 323, 116242, https://doi.org/10.1016/j.jenvman.2022.116242, 2022.

Li, T., Zeng, J., He, B., and Chen, Z.: Changes in soil C, N, and P concentrations and stoichiometry in karst trough valley area under ecological restoration: The role of slope aspect, land use, and soil depth, Forests, 12, 144, https://doi.org/10.3390/f12020144, 2021.

Libbey, K. and Hernández, D. L.: Depth profile of soil carbon and nitrogen accumulation over two decades in a prairie restoration experiment, Ecosystems, 24, 1348–1360, https://doi.org/10.1007/s10021-020-00588-3, 2021.

Liu, Z., Song, Y., Qin, X., Yuan, J., Lou, Y., Yang, C., Tang, H., and Song, C.: Deep soil microbial carbon metabolic function is important but often neglected: A study on

https://doi.org/10.5194/egusphere-2026-180
Preprint. Discussion started: 17 March 2026

631 the Songnen Plain reed wetland, Northeast China, Fundamental Research, 3, 833–843,
632 https://doi.org/10.1016/j.fmre.2022.06.013, 2022.
633 Lovley, D. R. and Phillips, E. J. P.: Novel mode of microbial energy metabolism:
634 Organic carbon oxidation coupled to dissimilatory reduction of iron or manganese,
635 Applied and Environmental Microbiology, 54, 1472–1480,
636 https://doi.org/10.1128/aem.54.6.1472-1480.1988, 1988.
637 Luo, S., Yuan, J., Song, Y., Ren, J., Qi, J., Zhu, M., Feng, Y., Li, M., Wang, B., Li, X.,
638 and Song, C.: Elevated salinity decreases microbial community complexity and
639 carbon, nitrogen and phosphorus metabolism in the Songnen Plain wetlands of China,
640 Water Research, 276, 123285, https://doi.org/10.1016/j.watres.2025.123285, 2025.
641 Murdiyarso, D., Krisnawati, H., Adinugroho, W. C., and Sasmito, S. D.: Deriving
642 emission factors for mangrove blue carbon ecosystem in Indonesia, Carbon Balance
643 and Management, 18, 22, https://doi.org/10.1186/s13021-023-00233-1, 2023.
644 Ni, B., Yu, X., Duan, X., and Zou, Y.: Wetland soil organic carbon balance is
645 reversed by old carbon and iron oxide additions, Frontiers in Microbiology, 14,
646 1327265, https://doi.org/10.3389/fmicb.2023.1327265, 2024.
647 Oren, A., Rotbart, N., Borisover, M., and Bar-Tal, A.: Chloroform fumigation
648 extraction for measuring soil microbial biomass: The validity of using samples
649 approaching water saturation, Geoderma, 318, 138–145,
650 https://doi.org/10.1016/j.geoderma.2018.01.007, 2018.
651 Peng, Y. J., Chahal, I., Hooker, D. C., and Van Eerd, L. L.: Comparison of equivalent
652 soil mass approaches to estimate soil organic stocks under long-term tillage, Soil
653 Tillage Research, 238, 106021, https://doi.org/10.1016/j.still.2024.106021, 2024.
654 Poulton, S. W. and Canfield, D. E.: Development of a sequential extraction procedure
655 for iron: Implications for iron partitioning in continentally derived particulates,
656 Chemical Geology, 214, 209–221, https://doi.org/10.1016/j.chemgeo.2004.09.003,
657 2005.
658 Rogers, K., Kelleway, J., Saintilan, N., Megonigal, J., Adams, J., Holmquist, J., Lu,
659 M., Lu, M., Schile-Beers, L., Zawadzki, A., Mazumder, D., and Woodroffe, C.:
660 Wetland carbon storage controlled by millennial-scale variation in relative sea-level

https://doi.org/10.5194/egusphere-2026-180
Preprint. Discussion started: 17 March 2026

661 rise, Nature, 567, 91–95, https://doi.org/10.1038/s41586-019-0951-7, 2019.
662 Rowland, P. I., Wartman, M., Bursic, J., and Carnell, P.: Restored and created tidal
663 marshes recover ecosystem services over time, Environmental and Sustainability
664 Indicators, 24, 100539, https://doi.org/10.1016/j.indic.2024.100539, 2024.
665 Vigneron, A., Alsop, E. B., Lomans, B. P., Kyrpides, N. C., Head, I. M., and
666 Tsesmetzis, N.: Succession in the petroleum reservoir microbiome through an oil field
667 production lifecycle, ISME Journal, 11, 2141–2154,
668 https://doi.org/10.1038/ismej.2017.78, 2017.
669 Wang, Q., Cui, G., Liu, H., Huang, X., Xiao, X., Wang, M., Jia, M., Mao, D., Li, X.,
670 Xiao, Y., and Li, H.: Spatiotemporal dynamics and potential distribution prediction of
671 Spartina alterniflora invasion in Bohai Bay based on Sentinel time-series data and
672 MaxEnt modeling, Remote Sensing, 17, 975, https://doi.org/10.3390/rs17060975,
673 2025.
674 Wang, X., Xia, X., Riaz, M., Babar, S., El-Desouki, Z., Qasim, M., Wang, J., and
675 Jiang, C.: Biochar amendment modulate microbial community assembly to mitigate
676 saline-alkaline stress across soil depths, Journal of Environmental Management, 385,
677 125574, https://doi.org/10.1016/j.jenvman.2025.125574, 2025.
678 Wang, X., Zhang, J., Yang, B., Mao, H., Yu, Q., and Zhang, Y.: Intermittent
679 microaeration enhanced anaerobic digestion: The key role of Fe(III)/Fe(II) cycle and
680 reactive oxygen species, Environmental Science & Technology, 59, 8629–8639,
681 https://doi.org/10.1021/acs.est.5c04187, 2025.
682 Wang, Y., Liu, X., Zhang, X., Dai, G., Wang, Z., and Feng, X.: Evaluating wetland
683 soil carbon stability related to iron transformation during redox oscillations,
684 Geoderma, 428, 116222, https://doi.org/10.1016/j.geoderma.2022.116222, 2022.
685 Wang, Y., Wang, H., He, J.-S., and Feng, X.: Iron-mediated soil carbon response to
686 water-table decline in an alpine wetland, Nature Communications, 8, 15972,
687 https://doi.org/10.1038/ncomms15972, 2017.
688 Wen, S., Chen, J., Yang, Z., Deng, L., Feng, J., Zhang, W., Zeng, X., Huang, Q.,
689 Delgado-Baquerizo, M., and Liu, Y.-R.: Climatic seasonality challenges the stability
690 of microbial-driven deep soil carbon accumulation across China, Global Change

https://doi.org/10.5194/egusphere-2026-180
Preprint. Discussion started: 17 March 2026

691 Biology, 29, 4430–4439, https://doi.org/10.1111/gcb.16760, 2023.
692 Wendt, J. W. and Hauser, S.: An equivalent soil mass procedure for monitoring soil
693 organic carbon in multiple soil layers, European Journal of Soil Science, 64, 58–65,
694 https://doi.org/10.1111/ejss.12002, 2013.
695 Wagai, R. and Mayer, K. U.: Iron-bound organic carbon in forest soils: Quantification
696 and characterization, Soil Biology and Biochemistry, 39, 2438–2452,
697 https://doi.org/10.1016/j.soilbio.2007.04.004, 2007.
698 Wu, B., Tang, X., Song, Z., Qi, M., Liu, M., Li, X., and Hou, L.: Chemoautotrophic
699 carbon fixation favors iron-bound organic carbon formation in estuarine and coastal
700 sediments, Environmental Science & Technology, 59, 12642–12655,
701 https://doi.org/10.1021/acs.est.5c00324, 2025.
702 Wu, L., Song, Z., Xiao, Z., Zhang, X., Van Zwieten, L., Guo, L., Li, Z., Yang, X.,
703 Zhao, X., Wang, Y., He, D., Wang, W., Liu, C., and Wang, H.: Assessment of soil
704 organic and inorganic carbon stocks in coastal salt marshes of China: key mechanisms
705 elucidated, Global Change Biology, 31, e70421, https://doi.org/10.1111/gcb.70421,
706 2025.
707 Xia, S., Song, Z., Van Zwieten, L., Guo, L., Yu, C., Wang, W., Li, Q., Hartley, I.,
708 Yang, Y., Liu, H., Wang, Y., Ran, X., Liu, C., and Wang, H.: Storage, patterns and
709 influencing factors for soil organic carbon in coastal wetlands of China, Global
710 Change Biology, 28, 6065–6085, https://doi.org/10.1111/gcb.16325, 2022.
711 Xiao, L., Zhang, W., Hu, P., Xiao, D., Yang, R., Ye, Y., and Wang, K.: The formation
712 of large macroaggregates induces soil organic carbon sequestration in short-term
713 cropland restoration in a typical karst area, Science of the Total Environment, 801,
714 149588, https://doi.org/10.1016/j.scitotenv.2021.149588, 2021.
715 Yang, R., Yang, S., Chen, L., Yang, Z., Xu, L., Zhang, X., Liu, G., Jiao, C., Bai, R.,
716 Zhang, X., Zhai, B., Wang, Z., Zheng, W., Li, Z., and Zamanian, K.: Effect of
717 vegetation restoration on soil erosion control and soil carbon and nitrogen dynamics:
718 A meta-analysis, Soil and Tillage Research, 230, 105705,
719 https://doi.org/10.1016/j.still.2023.105705, 2023.
720 Yang, Y., Zhao, Z., and Zhang, Y.: Anaerobic ammonium removal pathway driven by

https://doi.org/10.5194/egusphere-2026-180
Preprint. Discussion started: 17 March 2026

721 the Fe(II)/Fe(III) cycle through intermittent aeration, Environmental Science &
722 Technology, 55, 7615–7623, https://doi.org/10.1021/acs.est.0c08624, 2021.
723 Yu, C., Xie, S., Song, Z., Xia, S., and Åström, M. E.: Biogeochemical cycling of iron
724 (hydr-)oxides and its impact on organic carbon turnover in coastal wetlands: A global
725 synthesis and perspective, Earth-Science Reviews, 218, 103658,
726 https://doi.org/10.1016/j.earscirev.2021.103658, 2021.
727 Zhang, B., Xu, C., Zhang, Z., Hu, C., He, Y., Huang, K., Pang, Q., and Hu, G.:
728 Response of soil organic carbon and its fractions to natural vegetation restoration in a
729 tropical karst area, southwest China, Frontiers in Forests and Global Change, 6,
730 1172062, https://doi.org/10.3389/ffgc.2023.1172062, 2023.
731 Zhang, D., Cai, X., Diao, L., Wang, Y., Wang, J., An, S., Cheng, X., and Yang, W.:
732 Changes in soil organic carbon and nitrogen pool sizes, dynamics, and biochemical
733 stability during ~160 years natural vegetation restoration on the Loess Plateau, China,
734 Catena, 211, 106014, https://doi.org/10.1016/j.catena.2021.106014, 2022.
735 Zhang, G., Bai, J., Tebbe, C. C., Zhao, Q., Jia, J., Wang, W., Wang, X., and Yu, L.:
736 Salinity controls soil microbial community structure and function in coastal estuarine
737 wetlands, Environmental Microbiology, 23, 1020–1037,
738 https://doi.org/10.1111/1462-2920.15281, 2021.
739 Zhang, J., Zhao, S., Miao, Q., Feng, L., Chi, Z., Li, Z., Shuai, K., Chen, X., Liu, Y.,
740 Hu, R., Peng, G., Li, J., Hu, Y., Su, Z., Fang, M., and Li, J.: Effect of subsurface
741 drainage in regulating water on desalinization and microbial communities in salinized
742 irrigation soils, Agronomy, 14, 282, https://doi.org/10.3390/agronomy14020282,
743 2024.
744 Zhao, N., Ding, H., Zhou, X., Guillemot, T., Zhang, Z., Zhou, N., and Wang, H.:
745 Dissimilatory iron-reducing microorganisms: The phylogeny, physiology,
746 applications and outlook, Critical Reviews in Environmental Science and Technology,
747 55, 73–98, https://doi.org/10.1080/10643389.2024.2382498, 2025.
748 Zheng, B., Xiao, Z., Liu, J., Zhu, Y., Shuai, K., Chen, X., Liu, Y., Hu, R., Peng, G., Li,
749 J., Hu, Y., Su, Z., Fang, M., and Li, J.: Vertical differences in carbon metabolic
750 diversity and dominant flora of soil bacterial communities in farmlands, Scientific

https://doi.org/10.5194/egusphere-2026-180
Preprint. Discussion started: 17 March 2026

751 Reports, 14, 60142, https://doi.org/10.1038/s41598-024-60142-2, 2024.

752 Zheng, J., Sun, L., Zhong, L., Yuan, Y., Wang, X., Wu, Y., Lu, C., Xue, S., and Song,
753 Y.: Allometric growth and carbon sequestration of young Kandelia obovata
754 plantations in a constructed urban coastal wetland in Haicang Bay, Southeast China,
755 Forests, 16, 1126, https://doi.org/10.3390/f16071126, 2025.